

# Monte Carlo Renormalization Group Analysis of Lattice $\phi^4$ Model in $D = 3, 4$

M. Itakura

*Center for Promotion of Computational Science and Engineering, Japan Atomic Energy Research Institute, Meguro-ku, Nakameguro 2-2-54, Tokyo 153, Japan*  
(February 19, 2019)

## Abstract

We present a simple, sophisticated method to capture renormalization group flow in Monte Carlo simulation, which provides important information of critical phenomena. We applied the method to  $D = 3, 4$  lattice  $\phi^4$  model and obtained renormalization flow diagram which well reproduces theoretically predicted behavior of continuum  $\phi^4$  model. We also show that the method can be easily applied to much more complicated models, such as frustrated spin models.

PACS numbers: 20.70.Lq, 75.10.Hk

## I. INTRODUCTION

Renormalization group (RG) theory [1–4] has drastically improved perspective about phase transition. When it is combined with Monte Carlo (MC) simulation, it becomes very powerful tool to investigate critical phenomena. However, the so-called Monte Carlo Renormalization Group (MCRG) method [5–9] requires elaborated scheme and experience, and application has been restricted to simple models such as Ising ferromagnet to now. In this paper we re-formulate the MCRG method and present simple way to obtain RG flow diagram in MC simulation, which provides essential information about critical phenomena. This paper is organized as follows: In section II, problems in the conventional MCRG scheme is explained and remedies for each problems are presented. In fact, modification of the conventional scheme leads to use of Binder’s parameter [10] and the second parameter, which is used in recent high-precision numerical works [15,14]. In section III, expected behavior of RG flow in  $D = 4$  lattice  $\phi^4$  model is presented for comparison with the MC result. Some caution on MC simulation just at the upper critical dimension is also presented. In section IV, detail of MC simulation of lattice  $\phi^4$  model is described. In section V and VI, result of MC simulation for  $D = 3, 4$  is presented. In section VII, we summarize the result and discuss possible applications of the method to more complicated models.

## II. MODIFICATION OF THE CONVENTIONAL MCRG METHOD

In the conventional MCRG scheme [5–8], critical exponents are calculated from eigenvalues of the linearized RG transformation:

$$\frac{\partial K_i(L, b_1)}{\partial K_j(L, b_2)} \quad (1)$$

where  $K_i(L, b)$  denotes coupling strength of  $i$ ’th term of block-spin Hamiltonian with block size  $b$ , and  $L$  denotes original size of the system.

One problem is that one should use proper definition of block-spin, unless  $K_i(L, b)$  goes to zero or infinity as  $b$  become large even at the critical point. For Ising model, the majority rule is one of the options. However, it cannot extended to more complicated models. There are infinite kind of definition and location of the fixed point (along irrelevant direction) depends on it [6].

In this paper, we use one which seems most simple and suitable for Monte Carlo simulation:

$$\bar{s}_b \equiv s_b / \sqrt{< s_b^2 >}, \quad (2)$$

where  $s_b$  denotes summation of all spins in the block. This definition is implicitly used in the definition of Binder’s parameter. Actually, we use coarse-grained spin obtained by cutting high-momentum modes off, as in Ref. [9]. However, we set  $b = L$  at the last stage, therefore real-space RG and momentum-space RG don’t make much difference.

Another problem is that the block size  $b$  should be much smaller than  $L$ , unless the behavior of block-spin is affected by boundary condition which is non-universal. Thus one faces a trade-off that for larger  $b$ , behavior of block-spins become more asymptotic (couplings

of irrelevant terms become smaller) but their behavior deviates from bulk one. The solution is to use the following matrix

$$\frac{\partial K_i(bL, bL)}{\partial K_j(L, L)} = \frac{\partial K_i(bL, bL)}{\partial K_j(bL, b)} \cdot \frac{\partial K_i(bL, b)}{\partial K_j(bL, 1)} \cdot \left[ \frac{\partial K_i(L, L)}{\partial K_j(L, 1)} \right]^{-1}, \quad (3)$$

instead of (1). At critical point,

$$\frac{\partial K_i(bL, bL)}{\partial K_j(bL, b)} = \frac{\partial K_i(L, L)}{\partial K_j(L, 1)} \quad (4)$$

should be satisfied and eigenvalues of the matrix (3) coincide with that of (1). Thus one can use as large block-size as the system size.

Yet another, and most severe problem is referred as "redundancy problem" [7,8]. In the conventional MCRG scheme, one should observe very large number of block-spin interaction term to construct fixed-point Hamiltonian. However, in the continuum  $\phi^4$  theory, there are only two kinds of independent coupling constant (mass and coupling). Lattice Hamiltonian approaches this continuum one asymptotically after momentum-space RG transform, and two terms are enough to observe essential RG flow.

Let us consider the Hamiltonian defined on  $D$ -dimensional continuum space:

$$\mathcal{H} = \int d\mathbf{x} \left[ \frac{\gamma}{2} (\nabla \phi(\mathbf{x}))^2 + \frac{\alpha}{2} \phi(\mathbf{x})^2 + \beta \phi(\mathbf{x})^4 \right] \quad (5)$$

Note that it is not microscopic Hamiltonian: it is phenomenological Hamiltonian and the parameters  $\gamma, \alpha, \beta$  should be determined to reproduce experimental result. In other word, it is logarithm of probability of observing specific configuration of some physical quantity  $\phi(\mathbf{x})$  in experiment. This means that short length scale fluctuations beneath the resolution  $l$  of the observation device is already integrated out and absorbed into the parameters  $\gamma, \alpha, \beta$ . Thus parameters depend on the cut-off length  $l$  and should be denoted by  $\gamma_l, \alpha_l, \beta_l$ . We also denote the physical quantity  $\phi(\mathbf{x})$  averaged over a volume of linear length  $l$  by  $\phi_l(\mathbf{x})$ .

We replace the parameters in (5) by "regularized" one defined as follows:

$$\bar{\alpha}_l = l^D \langle \phi_l(x)^2 \rangle \alpha_l, \quad \bar{\beta}_l = l^D \langle \phi_l(x)^2 \rangle^2 \beta_l, \quad \bar{\gamma}_l = l^{D-2} \langle \phi_l(x)^2 \rangle \gamma_l.$$

In terms of this regularization, Hamiltonian is expressed as

$$\begin{aligned} & \int_{|\mathbf{p}| \leq \pi} d\mathbf{p} \frac{\bar{\alpha} + \bar{\gamma} \mathbf{p}^2}{2} \bar{\phi}(\mathbf{p}) \bar{\phi}(-\mathbf{p}) \\ & + \bar{\beta} \int_{|\mathbf{p}_i| < \pi} d\mathbf{p}_1 d\mathbf{p}_2 d\mathbf{p}_3 d\mathbf{p}_4 \delta\left(\sum_i \mathbf{p}_i\right) \bar{\phi}(\mathbf{p}_1) \bar{\phi}(\mathbf{p}_2) \bar{\phi}(\mathbf{p}_3) \bar{\phi}(\mathbf{p}_4), \end{aligned} \quad (6)$$

where  $\bar{\phi}(\mathbf{p}) \equiv \phi(\mathbf{p}l) \langle \phi_l^2 \rangle^{-1/2}$ . All possible value of regularized parameter falls on a two-dimensional manifold on which  $\langle \bar{\phi}_l(x)^2 \rangle = 1$  is satisfied. This regularization is suitable for MC, compared to the field theoretical one  $\gamma \equiv 1$ . Fig.1 and Fig.2 show schematic RG flow of these regularized parameters in  $D = 3$  and 4, respectively: high temperature, low temperature, Gaussian, and Wilson-Fisher fixed point is denoted by H,L,G, and WF, respectively.

Now let us return to the lattice model defined as follows:

$$H_L = \frac{\gamma}{2} \sum_{\langle ij \rangle} (s_i - s_j)^2 + \sum_i \frac{\alpha}{2} s_i^2 + \beta s_i^4. \quad (7)$$

where the summation  $\sum_{\langle ij \rangle}$  sums over all nearest neighbor pairs. If we apply momentum-space RG transform of factor  $b$  to (7), renormalized Hamiltonian takes the following form:

$$H(L, b) = \frac{\bar{\alpha}(L, b)}{2} (L/b)^{-D} \sum_{|\mathbf{p}| \leq \pi}^{(L/b)} \bar{s}_b(\mathbf{p}) \bar{s}_b(-\mathbf{p}) \quad (8)$$

$$+ \frac{\bar{\gamma}(L, b)}{2} (L/b)^{-D} \sum_{|\mathbf{p}| \leq \pi}^{(L/b)} \mathbf{p}^2 \bar{s}_b(\mathbf{p}) \bar{s}_b(-\mathbf{p}) \quad (9)$$

$$+ \bar{\beta}(L, b) (L/b)^{-3D} \sum_{\substack{|\mathbf{p}_i| \leq \pi \\ \mathbf{p}_1 + \mathbf{p}_2 + \mathbf{p}_3 + \mathbf{p}_4 = 0}}^{(L/b)} \bar{s}_b(\mathbf{p}_1) \bar{s}_b(\mathbf{p}_2) \bar{s}_b(\mathbf{p}_3) \bar{s}_b(\mathbf{p}_4), \quad (10)$$

where  $\bar{s}_b(\mathbf{p}) = s(b\mathbf{p}) < s_b^2(x) >^{-1/2}$  and the symbol  $\sum_{\mathbf{p}}^{(N)}$  denotes summation over  $0, \pm 2\pi/N, \pm 4\pi/N, \dots$  for each components of  $\mathbf{p}$ ,  $s(\mathbf{p})$  denotes Fourier components of  $s_i$  and

$$s_b(\mathbf{x}) = (L/b)^{-D} \sum_{|\mathbf{p}| \leq \pi/b} e^{i\mathbf{p} \cdot \mathbf{x}} s(\mathbf{p}) \quad (11)$$

is coarse-grained spin at  $\mathbf{x}$ . Actually, higher terms such as  $O(\bar{s}_b^6)$  are present in  $H(L, b)$  but they vanish as  $L$  and  $b$  become large.

Note that  $< \sum_{\mathbf{p}} \bar{s}_b(\mathbf{p}) \bar{s}_b(-\mathbf{p}) > = \text{const}$  by definition and there are only two kinds of interesting terms. If we set  $b = L$ , the term (10) is exactly the Binder's parameter and we denote it by  $B_L$ . The term (9) vanishes if we set  $b = L$ , so we must stop RG transform at  $b = L/2$ . Then it becomes

$$\frac{2\pi^2 < s(\mathbf{k}_1) s(-\mathbf{k}_1) >}{2^{-D} < s(0)^2 + 2s(\mathbf{k}_1) s(-\mathbf{k}_1) >} \quad (12)$$

where  $\mathbf{k}_1 \equiv (2\pi/L, 0, \dots, 0)$ . For simplicity, we use the following quantity:

$$C_L \equiv \frac{< s(\mathbf{k}_1) s(-\mathbf{k}_1) >}{< s^2(0) >}. \quad (13)$$

Recently, several different parameters have been proposed as the second parameter  $C_L$  to estimate and eliminate sub-leading scaling field. We will review these works in the next subsection.

Now consider the following matrix:

$$\frac{\partial(B_{bL}, C_{bL})}{\partial(B_L, C_L)} = \frac{\partial(B_{bL}, C_{bL})}{\partial(\bar{\beta}_1, \bar{\gamma}_1)} \cdot \left( \frac{\partial(B_L, C_L)}{\partial(\bar{\beta}_1, \bar{\gamma}_1)} \right)^{-1} \quad (14)$$

$$= \frac{\partial(B_{bL}, C_{bL})}{\partial(\bar{\beta}_b, \bar{\gamma}_b)} \cdot \frac{\partial(\bar{\beta}_b, \bar{\gamma}_b)}{\partial(\bar{\beta}_1, \bar{\gamma}_1)} \cdot \left( \frac{\partial(B_L, C_L)}{\partial(\bar{\beta}_1, \bar{\gamma}_1)} \right)^{-1}. \quad (15)$$

instead of

$$\frac{\partial[\bar{\beta}(bL, bL), \bar{\gamma}(bL, bL/2)]}{\partial[\bar{\beta}(L, L), \bar{\gamma}(L, L/2)]}. \quad (16)$$

At the fixed point,

$$\frac{\partial(B_L, C_L)}{\partial(\bar{\beta}_1, \bar{\gamma}_1)} = \frac{\partial(B_{bL}, C_{bL})}{\partial(\bar{\beta}_b, \bar{\gamma}_b)} \quad (17)$$

is satisfied and eigenvalues of  $\partial(B_{bL}, C_{bL})/\partial(B_L, C_L)$  coincide with that of  $\partial(\bar{\beta}_b, \bar{\gamma}_b)/\partial(\bar{\beta}_1, \bar{\gamma}_1)$  as long as  $\partial(B_L, C_L)/\partial(\bar{\beta}_1, \bar{\gamma}_1)$  is non-singular matrix.

Thus scaling behavior of renormalized parameters can be extracted from that of  $(B_L, C_L)$ , as long as  $|\partial(B_L, C_L)/\partial(\bar{\beta}_1, \bar{\gamma}_1)| \neq 0$ : If we draw arrows from  $(B_L, C_L)$  to  $(B_{bL}, C_{bL})$  in  $B_L - C_L$  plane, renormalization flow diagram of factor  $b$  is obtained. From this diagram, one can determine whether MC result is asymptotic enough or not, by checking whether  $(B_L, C_L)$  converge to a fixed point. When sub-leading scaling field is expected to be very large, such as in the recent Monte Carlo studies of 5D Ising model [11–13], this RG flow diagram is very useful compared to many parameter fit to single observable  $B_L$ .

Linearized RT matrix  $\mathbf{R}_b = \partial(B_{bL}, C_{bL})/\partial(B_L, C_L)$  is calculated, for example, from linear fitting

$$\begin{pmatrix} B_{bL}(\alpha, \beta, \gamma) \\ C_{bL}(\alpha, \beta, \gamma) \end{pmatrix} = \mathbf{R}_b \cdot \begin{pmatrix} B_L(\alpha, \beta, \gamma) \\ C_L(\alpha, \beta, \gamma) \end{pmatrix} + \begin{pmatrix} B_0 \\ C_0 \end{pmatrix} \quad (18)$$

where  $\mathbf{R}_b$  and  $(B_0, C_0)$  are fitting parameters and we use values of  $(B_L, C_L)$  and  $(B_{bL}, C_{bL})$  at several different parameter  $\alpha, \beta, \gamma$  near the fixed point. Selection of this parameter is delicate problem: when it is too close to the fixed point,  $(B_L, C_L)$  and  $(B_{bL}, C_{bL})$  become very close to each other and RG flow is buried in statistical errors, while when it is far from the fixed point, non-linear dependence of  $(B_L, C_L)$  on  $(\alpha, \beta, \gamma)$  induces systematic error. Thus the parameter range for the fitting should be determined carefully.

Of course  $\mathbf{R}_b$  can be calculated from  $\alpha, \beta, \gamma$ -derivatives of  $B_L$  and  $C_L$  at the fixed point. However, derivative with respect to irrelevant direction vanish as  $L$  become large and buried in statistical errors. Thus values of  $B_L, C_L$  at parameters well apart from the fixed point along irrelevant direction are needed to calculate the second eigenvalue.

### A. The second parameter in literature

In this subsection, we compare our definition of  $C_L$ , “the second parameter” (the first one is the Binder’s parameter), with preceding works.

Ballesteros *et.al.* [14] used finite size correlation length defined as below

$$\xi^2 \equiv \frac{<\phi(0)^2> / <\phi(\mathbf{k}_1)\phi(-\mathbf{k}_1)> - 1}{\sin^2(|\mathbf{k}_1|)}, \quad (19)$$

which is related to  $C_L$  as  $\xi^2 \sin^2(|\mathbf{k}_1|) = -1 + 1/C_L$ .

Hasenbusch [15] used ratio between partition function of periodic and anti-periodic Hamiltonian. In momentum representation, Hamiltonian for anti-periodic boundary condition (APBC) is obtained by replacing  $\mathbf{k}$  summation of the lattice Hamiltonian by  $k_\mu = \pm\pi/L, \pm 3\pi/L, \dots$  for each direction  $\mu$  to which APBC is imposed. Let us denote partition function of periodic and anti-periodic Hamiltonian by  $Z_p$  and  $Z_a$ , respectively. Then it reads:

$$Z_a/Z_p = \frac{\int \mathcal{D}\phi \exp(-H_a)}{\int \mathcal{D}\phi \exp(-H_p)} \quad (20)$$

$$= \frac{\int \mathcal{D}\phi \exp(-H_p) \exp(H_p - H_a)}{\int \mathcal{D}\phi \exp(-H_p)} = \langle \exp(H_p - H_a) \rangle_p \quad (21)$$

where  $H_p$  and  $H_a$  denote periodic and anti-periodic Hamiltonian, respectively,  $\langle \dots \rangle_p$  denotes average with respect to  $H_p$ . When APBC is imposed to a direction of  $\mathbf{e}_1$ , it reads

$$H_a - H_p \sim \sum_{\mathbf{k}} \frac{2\pi|k_1|}{L} \phi(\mathbf{k})\phi(-\mathbf{k}) \quad (22)$$

for large  $L$ . One can see that  $Z_a/Z_p$  has similar form as that of  $C_L$ . In the real-space RG scheme, both  $C_L$  and  $Z_a/Z_p$  can be regarded as an effective coupling between two block-spins defined on  $L \times L \times \dots \times L/2$  block.

### III. PERTURBATION EXPANSION AT $D = 4$

Near the Gaussian fixed point, finite-size behavior of  $B_L$  and  $C_L$  can be predicted from finite-size perturbation theory proposed by Chen and Dohm [16]. Note that, when  $D = 4$ , there is one kind of divergent sub-diagram (Fig.3) whose factor is proportional to  $[\beta_1(C_0 + C_1 \log L)/\gamma_1^2]$  at the critical region, where  $C_0, C_1 > 0$  are some constants. Thus perturbation is restricted to the range  $\beta_1(C_0 + C_1 \log L)/\gamma_1^2 \ll 1$  and one cannot set  $L \rightarrow \infty$ . However, limit for  $L$  rapidly diverge as we approach the Gaussian fixed point, and good agreement between perturbation theory and Monte Carlo data is expected for certain parameter range and lattice size. Then one can predict scaling behavior for large  $L$ , which is far beyond the computational limit of Monte Carlo simulation, from the perturbation theory.

Here we investigate finite-size behavior of  $B_L$  and  $C_L$  at the finite-size critical point (to one-loop order):

$$\alpha = -12 \frac{\beta}{\gamma} L^{-D} \sum_{\mathbf{k} \neq 0} \frac{1}{2J(\mathbf{k})} \quad (23)$$

where  $J(\mathbf{k}) = \sum_\mu (1 - \cos k_\mu)$ .

$B_L$  takes so-called zero-mode value:

$$B_{\text{ZM}} \equiv \frac{\int d\Phi_0 \exp(-\Phi_0^4) \Phi_0^4 / \int d\Phi_0 \exp(-\Phi_0^4)}{\left[ \int d\Phi_0 \exp(-\Phi_0^4) \Phi_0^2 / \int d\Phi_0 \exp(-\Phi_0^4) \right]^2} \approx 2.1844. \quad (24)$$

As for  $C_L$ , to one-loop order,

$$C_L = \frac{\sqrt{\beta}}{8\pi^2\gamma} \sqrt{1 - 36\frac{\beta}{\gamma^2} \sum_{\mathbf{k} \neq 0} [2J(\mathbf{k})]^{-2}}. \quad (25)$$

For large  $L$ ,  $\sum_{\mathbf{k} \neq 0} [2J(\mathbf{k})]^{-2} \sim A_1 + A_2 \log L$  where  $A_1$  and  $A_2$  are some positive constant. Thus plot of  $(B_L, C_L)$  for certain range of parameter including critical temperature approaches  $(B_{\text{ZM}}, 0)$  as  $L$  increases or  $\beta$  decreases, indicating that the Gaussian fixed point is infrared-stable. However, approach to the point  $(B_{\text{ZM}}, 0)$  for increasing  $L$  is extremely slow, and one cannot expect asymptotic Gaussian behavior in MC simulations, even when  $L$  is very large. Critical exponents estimated from MC result may also differ from the Gaussian (classical) value and depend on the bare parameters. Thus one can extract only very restricted information from MC at the upper critical dimension.

#### IV. DETAIL OF MONTE CARLO SIMULATION

We investigated  $L \times L \times L$  system with  $L = 8, 16, 32$  for  $D = 3$  and  $L \times L \times L \times L$  system with  $L = 4, 8, 16$  for  $D = 4$ , imposing periodic boundary condition on each directions.

We used the following Hamiltonian:

$$H = \frac{\gamma}{2} \sum_{\langle ij \rangle} (s_i - s_j)^2 + \frac{\alpha}{2} \sum_i s_i^2 + \beta \sum_i s_i^4 \quad (26)$$

where  $-\infty < s_i < \infty$  denotes the spin on the site  $i$ . Since we cannot use the regularization condition  $\langle s_i^2 \rangle = 1$  before the simulation, we used the following one

$$\frac{\int d\phi \exp(-\frac{\alpha}{2}\phi^2 - \beta\phi^4)\phi^2}{\int d\phi \exp(-\frac{\alpha}{2}\phi^2 - \beta\phi^4)} = 1.$$

We used several fixed  $\alpha, \beta$  and tuned  $\gamma$  to reach the critical region. Actual values of parameters are listed in the later sections.

For parameters well apart from the Gaussian fixed point,  $4L^{D-2}$  single cluster flips [17] and 16 Metropolis sweeps are performed between successive observations. In the cluster-update stage, length of  $s_i$  is kept fixed and only its sign is changed. In the Metropolis update step, new value for  $s_i$  is chosen uniformly from a range  $\exp(-\alpha s^2 - \beta s^4) \geq \exp(-3.0)$ . By the cluster update, every spins are flipped four times on average between observations. For all observed quantities, correlation coefficient between successively observed values were less than 0.2.

As we approach the Gaussian fixed point, parameters behave as follows:

$$\alpha \sim 0, \quad \beta \sim \text{const}, \quad \gamma \rightarrow \infty. \quad (27)$$

Thus the nearest neighbor coupling  $\gamma s_i s_j / 2$  tends to diverge. Since the bond-cutting probability of the Wolff's algorithm is  $\exp(-\gamma s_i s_j)$ , cluster update tends to end up with flipping the whole system and does not accelerate the simulation. In these cases we increased the number of Metropolis sweeps until the above mentioned condition is satisfied.

Thermal averages of observables at  $\gamma$  slightly away from actually used value were calculated using reweighting techniques [18]. For all system sizes, at least  $0.8 \times 10^5$  observations were done after thermalization, and statistical errors were estimated by the jackknife procedure. Multiplicative lagged Fibonacci sequence  $R_t = R_{t-9689} \times R_{t-4187} \pmod{2^{31}}$  was used as a random number generator. All runs were performed on VPP-300 at JAERI.

## V. RESULT FOR $D = 3$

Simulations were performed at the following parameters (see also Fig. 4) for  $L = 8, 16, 32$ :

**Ising case:**  $\phi(\mathbf{x}) = \pm 1$ ,  $\gamma = 0.2217$ ,

**case A:**  $\alpha/2 = -2.6159$ ,  $\beta = 1.0948$ ,  $\gamma = 0.3040$ ,

**case B:**  $\alpha/2 = -1.6655$ ,  $\beta = 0.6935$ ,  $\gamma = 0.3545$ ,

**case C:**  $\alpha/2 = -0.8786$ ,  $\beta = 0.3938$ ,  $\gamma = 0.4700$ ,

**case D:**  $\alpha/2 = -0.5209$ ,  $\beta = 0.2713$ ,  $\gamma = 0.6260$ .

Fig.5 shows RG flow diagram of  $B_L$  and  $C_L$  near the Wilson-Fisher RG fixed point. All lines are drawn from  $(B_L, C_L)$  to  $(B_{2L}, C_{2L})$ . Dashed and solid lines correspond to  $L = 8$  and  $L = 16$ , respectively. One can see that the RG flow shown in Fig (1) is well reproduced. Moreover, linear fitting procedure (18) provides estimate for critical exponents as  $\nu = 0.69(3), \omega = 0.74(10)$  from  $L = 8, 16$  data and  $\nu = 0.653(10), \omega = 0.7(2)$  from  $L = 16, 32$  data, which is in agreement with most recent  $\epsilon$ -expansion result  $\nu = 0.6305(25), \omega = 0.814(10)$  [19] and Monte Carlo result  $\nu = 0.6296(3), \omega = 0.845(10)$  [15]. Thus one can see that the two observables  $B_L$  and  $C_L$  are enough to capture the essential RG flow.

## VI. RESULT FOR $D = 4$

Simulations were performed at the following parameters:

**Ising case:**  $\phi(\mathbf{x}) = \pm 1$ ,  $\gamma_1 = 0.1495$ ,

**case A:**  $\alpha/2 = -0.3226$ ,  $\beta = 0.2082$ ,  $\gamma = 0.54$ ,

**case B:**  $\alpha/2 = -0.1383$ ,  $\beta = 0.1530$ ,  $\gamma = 1.0$

for  $L = 4, 8$  and  $16$ . Near the Gaussian fixed point (case B), there are severe critical slowing-down (owing to large fluctuation of  $\mathbf{k} = 0$  mode) which cannot be removed by the cluster update and we did not perform  $L = 16$  simulation. For the case B, perturbation expansion agrees well with the MC result: Fig.6(a) and 6(b) show plot of  $B_L$  and  $C_L$ , respectively, against  $\gamma_1$  for fixed  $(\alpha, \beta)$ , together with perturbation results. Note that there are no free parameters to be fitted, unlike Ising case [20], and the agreement is both qualitative and quantitative.

Fig.7 shows RG flow diagram of  $B_L$  and  $C_L$  obtained from MC. All lines are drawn from  $(B_L, C_L)$  to  $(B_{2L}, C_{2L})$ . Dashed and solid lines correspond to  $L = 4$  and  $L = 8$ , respectively.

Simulations at a parameter closer to the Gaussian fixed point than case B is very hard owing to aforementioned critical slowing-down. Instead, finite-size perturbation provides reliable result near the Gaussian fixed point and it indicate that the plot of  $(B_L, C_L)$  approaches the Gaussian fixed point as  $L$  increase. Thus one can conclude that there is no RG fixed point except for the infrared-stable Gaussian fixed point.

## VII. CONCLUSION

Renormalization Group flow diagram obtained by the method presented in this paper provides qualitative information such as stability of specific RG fixed point against some perturbation, as well as quantitative improvement of estimated value of critical exponent by eliminating leading correction-to-scaling terms. However, in lattice models, there exists  $O(1/L)$  systematic error owing to the substitution of integral by finite summation of  $1/L$  mesh, and one cannot get rid of this as long as finite lattice system is concerned.

Our method can be easily extended to  $\phi^4$  models with several or unusual quartic coupling constant(s):

$$H = \int dx (\nabla \phi)^2 + \alpha \phi^2 + \sum_n \beta_n \sum_{ijkl} C_{ijkl}(n) \phi_i \phi_j \phi_k \phi_l, \quad (28)$$

such as chiral  $O(2n)$  model of triangular antiferromagnet [21], and Ginzburg-Landau model of type II superconductor under weak or strong magnetic field, with or without point/columnar impurities ( see [22,23] for transition of pure system under strong field). Multiple quartic term tend to generate irrelevant operator whose correction exponent is very small, making it difficult to observe asymptotic behavior in MC. Thus critical behavior of these models has been controversial issue and application of the MCRG method to these models seems very interesting. RG flow diagram of regularized quartic terms  $\langle C_{ijkl}(n) \phi_i \phi_j \phi_k \phi_l \rangle / \langle \sum_i \phi_i^2 \rangle^2$  will reveal the critical behavior, as in Ref. [24] of  $Q = 4$  antiferromagnetic Potts model.

Another important problem is estimation of correction exponent for  $\phi^6$  term at the WF fixed point. An  $\epsilon$  expansion analysis indicates that it become positive at the WF fixed point [4]. However, whether it is larger or smaller than  $\omega \approx 0.8$  of  $\phi^4$  theory, which we assumed as a *leading* correction, should be confirmed numerically. Similarly, effect of six-fold anisotropy on the critical behavior of 3D XY model is another interesting subject since the anisotropy is expressed by  $O(\phi^6)$  term.

## REFERENCES

- [1] L.P.Kadanoff, *Phisics* **2**, 263 (1966).
- [2] K.G.Wilson and J.Kogut, *Phys. Rep.* **12C**, 75 (1974).
- [3] D. J. Amit, *Field Theory, the Renormalization Group and Critical Phenomena*, 2nd. ed. (World Scientific 1984).
- [4] J. J. Binney, N. J. Dowrick, A. J. Fisher and M. E. J. Newman, *The Theory of Critical Phenomena* (Oxford University Press, Oxford, 1992).
- [5] R.H.Swendsen, *Phys. Rev. Lett.* **42**, 859 (1979).
- [6] H. W. J. Blöte, J. R. Heringa, A. Hoogland, E. W. Meyer, and T. S. Smit, *Phys. Rev. Lett.* **76**, 2613 (1996).
- [7] G. S. Pawley, R. H. Swendsen, D. J. Wallace, and K. G. Wilson, *Phys. Rev. B* **29**, 4030 (1984).
- [8] C. F. Baillie, R. Gupta, K. A. Hawick, and G. S. Pawley, *Phys. Rev. B* **45**, 10438 (1992).
- [9] D.Espriu and A.Travesset, *Phys. Lett.* **B356**, 329 (1995).
- [10] K. Binder, *Z. Phys. B* **43**, 119 (1981).
- [11] E.Luijten and H.W.J. Blöte, *Phys. Rev. Lett.* **76**, 1557 (1996); *ibid.* **76**, 3662 (1996); H.W.J. Blöte and E.Luijten, *Europhys.Lett.* **38**, 565 (1997); E.Luijten, *Europhys.Lett.* **37**, 489 (1997).
- [12] K.K.Mon, *Europhys.Lett.* **34**, 399 (1996); *ibid.* **37**, 493 (1997).
- [13] G.Parisi and J.J.Ruiz-Lorenzo, *Phys. Rev. B* **54**, R3698 (1996); **55**, 6082 (1997).
- [14] H.G.Ballesteros, L.A.Fernandez, V.Martin-Mayor and A. Munoz-Sudupe, *Phys. Lett. B* **441**, 330 (1998).
- [15] M.Hasenbusch, *J.Phys.A* **32**, 4851 (1999).
- [16] X.S.Chen and V.Dohm, *Int.J.Mod.Phys. C* **9**, 1073 (1998).
- [17] U. Wolff, *Phys. Rev. Lett.* **62**, 361 (1989).
- [18] A. M. Ferrenberg and R. H. Swendsen, *Phys. Rev. Lett.* **61**, 2635 (1988).
- [19] R.Guida and J.Zinn-Justin, *J.Phys.A* **31**, 8103 (1998).
- [20] E.Luijten, K.Binder, and H.W.J. Blöte, *Eur. Phys. J. B* **9**, 289 (1999).
- [21] H.Kawamura, *J.Phys.Condens.Matter* **10**, 4707 (1998).
- [22] E.Brezin,D.R.Nelson, and A.Thiaville, *Phys.Rev. B* **31**,7124 (1985).
- [23] X.Hu, S.Miyashita, and M.Tachiki, *Phys.Rev.Lett.* **79**,3498 (1997).
- [24] M. Itakura, *Phys. Rev. B* **60**, 6558 (1999).

## FIGURES

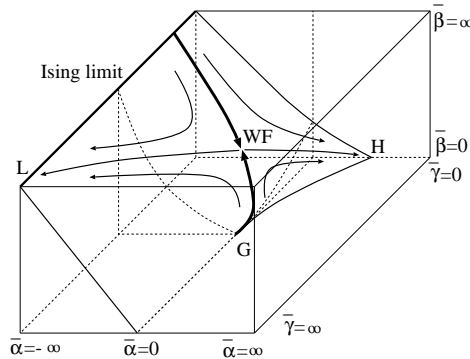


FIG. 1. Renormalization flow of regularized parameter in  $D = 3$ .

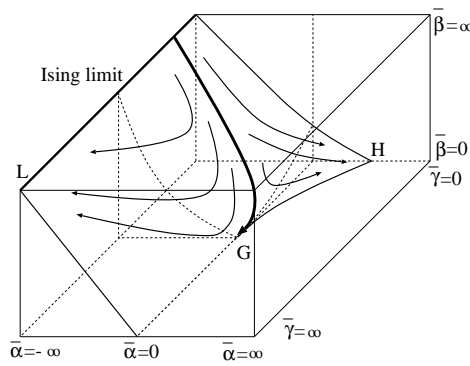


FIG. 2. Renormalization flow of regularized parameter in  $D = 4$ .

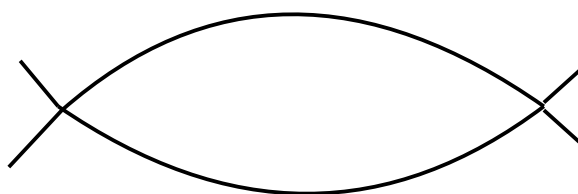


FIG. 3. Divergent sub-diagram in  $D = 4$ .

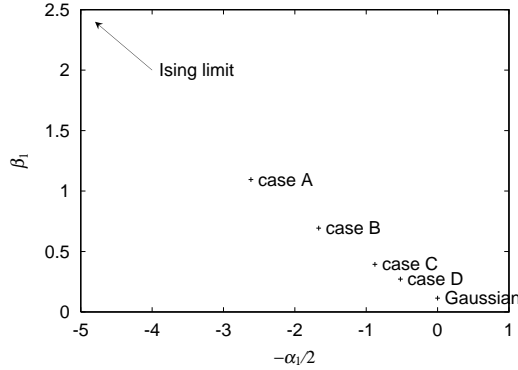


FIG. 4. Parameters at which simulations were performed.

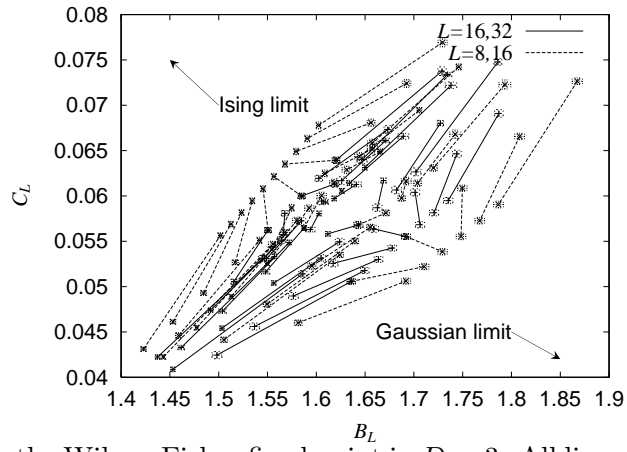


FIG. 5. RG flow near the Wilson-Fisher fixed point in  $D = 3$ . All lines are drawn from  $(B_L, C_L)$  to  $(B_{2L}, C_{2L})$ .

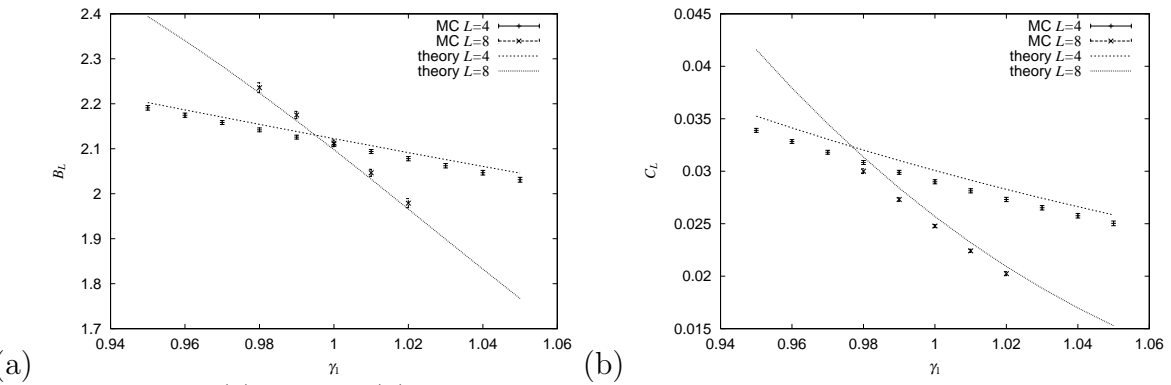


FIG. 6. Plot of (a)  $B_L$  and (b)  $C_L$  against  $\gamma_1$  for the case B in  $D = 4$ . ‘MC’ denotes Monte Carlo result and ‘theory’ denotes finite-size perturbation result.

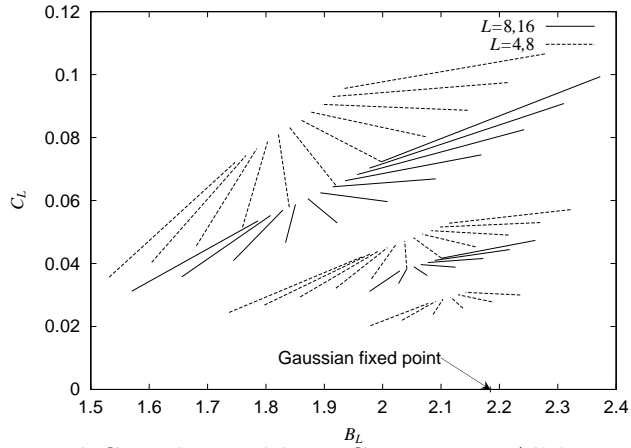


FIG. 7. RG flow of  $B_L$  and  $C_L$ , obtained by MC in  $D = 4$ . All lines are drawn from  $(B_L, C_L)$  to  $(B_{2L}, C_{2L})$ . Dashed and solid lines correspond to  $L = 4$  and  $L = 8$ , respectively.